IEEE Access
Multidisciplinary ⋮ Rapid Review ⋮ Open Access Journal

Received November 11, 2020, accepted November 19, 2020, date of publication November 25, 2020,
date of current version December 10, 2020.

Digital Object Identifier 10.1109/ACCESS.2020.3040394

A 0.3 THz Multi-Beam Extended Interaction Klystron Based on $TM_{10,1,0}$ Mode Coaxial Coupled Cavity

FU-MIN LIN, SHUNING WU, YUJIE XIAO, AND LIANGXIAN ZHANG
School of Physics and Optoelectronic Engineering, Guangdong University of Technology, Guangzhou 510006, China

Corresponding author: Fu-Min Lin (linfumin@gdut.edu.cn)

This work was supported in part by the Guangdong Science and Technology Program under Grant 2016A010101024, and in part by the Guangzhou Science and Technology Program under Grant 201802020003.

ABSTRACT A new conceive of high-order mode multi-beam Extended interaction Klystron (EIK) at the terahertz (THz) band is proposed. The interaction circuit based on the coaxial coupled cavity at $TM_{10,1,0}$-2π mode is designed and analyzed. Benefiting from the larger transverse space of the coaxial coupled cavity operating at high-order mode, multiple electron beams are formatted to reduce the current density of each electron beam. The crucial parameters associated with the interaction are determined by theoretical calculation and optimized by three-dimensional (3D) Particle-in-Cell (PIC) simulation. The results of theoretical analysis and PIC simulation demonstrate that the EIK operates at $TM_{10,1,0}$-2π mode without mode competition and self-oscillation. Driven by ten individual electron beams with the voltage of 20 kV, the current of 0.1 A and the current density of 318 A/cm^2, the maximum gain of 48 dB is achieved at the center frequency of 300 GHz with a 3-dB gain bandwidth of 200 MHz. And the corresponding output power and efficiency are 312.5 W and 1.56 %. The results indicate that the proposed EIK is a practical approach to generate high power terahertz waves using the thermal beam with a low compression ratio.

INDEX TERMS Terahertz, extended interaction klystron, high-order mode, multi-beam, coaxial coupled cavity, PIC simulation.

I. INTRODUCTION

The extended interaction device is a kind of vacuum electron device with high power, efficiency and reliability at millimeter and sub-millimeter wave frequencies, including Extended interaction Klystron (EIK) and Extended interaction Oscillator (EIO). Benefiting from the development of micro-fabrication technology and electronic optics technology, the extended interaction devices have been put into the applications that require excellent performance, ehigh stability and compact dimensions, such as satellite communication and the space-born radar [1]–[4]. However, there are many challenges in developing the extended interaction device at the terahertz band, the other factors such as conductivity, electron velocity spread and thermal dissipation become more significant than at lower frequencies [5], [6]. In addition, the dimension of the device decreases rapidly while the frequency increases to the terahertz band, which enormously increases the precision requirements of fabrication. The planar interaction circuits for millimeter wave EIKs such as ladder-type circuits and folded waveguides, are expected to be expanded to THz band, due to the promotion of high precision fabrication technology including Wire Electrical Discharge Machining (WEDM), lithographic (LIGA) and Nano Computer Numerical Control (CNC) milling [7], [8]. Moreover, the ladder-type extended interaction cavity operating at high-order mode is a potential solution [9].

Therefore, current challenges about the micro-fabrication of interaction circuits are perhaps trumped by the difficulties in producing small diameter, high current electron beams [5]. For a practical beam optics system optimized for a lifetime and electrical stresses, the current density emitted from the cathode must be kept within a reasonable range, and the compression of the beam is also limited. Thus, the beam current is inevitably restricted, which results in a significant reduction in output power and efficiency. One solution is to

The associate editor coordinating the review of this manuscript and approving it for publication was Giovanni Angiulli.

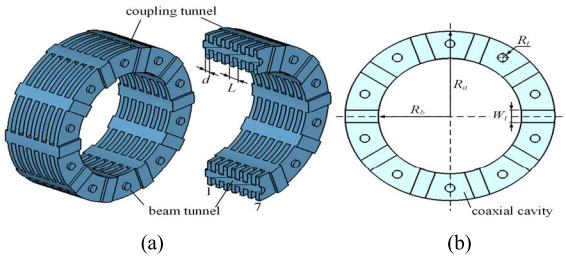

FIGURE 1. (a) Schematic of the $TM_{10,1,0}$ mode coaxial coupled cavity with seven structural periods. (b) cross section of the cavity.

develop the sheet beam devices that are expected to break the limitation of beam current and raise the power level[10]–[12]. However, the propagation of the electromagnetic waves in the beam tunnel is difficult to be cut off completely, which causes the signal feedback between cavities and results in the undesired oscillation. Another potential approach is to use the multi-beam interaction system to reduce the current density of beams [13], [14].

In this paper, a new type of EIK operating at $TM_{10,1,0-}2\pi$ mode with ten electron beams is proposed to overcome the above restrictions. Compared with the conventional EIKs operating at fundamental mode, the proposed high-order mode EIK has a large structure to accommodate multiple beams, which is expected to reduce the current density of the beams and suitable for the present technology of the cathode.The current density of the electron beam is very high, and the current density of the cathode does not reach the current density of the electron beam. In Sec. II, the high-order mode interaction circuit including the coaxial coupled cavity and the multi-extraction output cavity with axial output circuit are designed, and their crucial parameters associate with the interaction are analyzed and determined. In Sec. III, the possibilities of mode competition and self-oscillation are evaluated. The main performances and the power capability of the proposed EIK are demonstrated by 3D PIC simulation in Sec. IV. Conclusions and discussions are given in Section V.

II. INTERACTION CIRCUIT DESIGN

A. HIGH-ORDER MODE COUPLED CAVITY

The schematic of high-order mode coaxial coupled cavity with seven structural periods that is used as the bunching cavity is shown in Fig. 1, The cavity material is Oxygen-free copper, the main parameters of the coupled cavity are listed in TABLE 1. The coupled cavity consists of

seven coaxial cavities, which are coupled periodically by ten coupling tunnels. In general, the higher order mode has a higher frequency in the same cavity, in other words, at the same resonant frequency, the cavity operating at higher order mode has a larger dimension than that operating at the lower order mode. Therefore, the $TM_{10,1,0}$ mode is selected as the transverse operating mode in pursuit of a larger dimension. In order to maintain the phase consistency of the axial electric

TABLE 1. Parameters of coupled cavity.

Symbol	Quantity	Value
d	gap length	0.12 mm
L	period length	0.272 mm
W_t	width of coupling tunnel	0.4 mm
R_a	outer radius	2.648 mm
R_b	beam radius	1.8 mm
R_t	radius of beam tunnel	0.12 mm
f_r	resonant frequency	300 GHz
R/Q	characteristic impedance	18 Ω
Q_0	intrinsic quality factor	1100

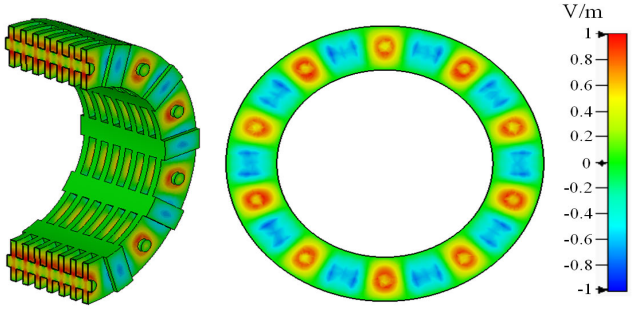

FIGURE 2. Normalized axial electric field pattern of $TM_{10,1,0-}2\pi$ mode at 300 GHz.

field in each period of the coupled cavity, the 2π mode is selected as the longitudinal operating mode. The axial electric field pattern of $TM_{10,1,0-}2\pi$ at 300 GHz is given by electromagnetic (EM) simulation using CST-MWS solver, as shown in Fig.2. According to the field pattern, ten cylindrical beam tunnels are arranged in where the axial electric field is extreme.

The gap coupling coefficient is an important parameter that reflects the interaction between the electron beam and the field. The case of a single gap is firstly considered. Because of the non-reentrant beam tunnel and the narrow gap, the amplitude of the axial electric field in the gap is approximately equal at any position. Referring to the research of [22], the square of the coupling coefficient M of a single gap is defined as

$$M^2 = M_Z^2 M_r^2 = \left[\frac{\sin\left(\theta_d/2\right)}{\theta_d/2}\right]^2 \frac{I_0^2\left(\gamma_e R_b\right) - I_1^2\left(\gamma_e R_b\right)}{I_0^2\left(\gamma_e R_t\right)} \quad (1)$$

where

$$\begin{cases} \theta_d = \beta_e d = \dfrac{\omega}{v_0} d \\ \gamma_e = \sqrt{\beta_e - k^2} = \sqrt{\left(\omega/v_0\right)^2 - \left(\omega/c\right)^2} \end{cases} \quad (2)$$

where M_z is the axial coupling coefficient; M_r is the radial coupling coefficient; θ_d is the gap transit angle; β_e is the longitudinal propagation constant of the beam; γ_e is the radial propagation constant of the beam; I_0 and I_1 are 0^{th}-order and 1^{st}-order first kind modified Bessel-functions, respectively; V_0 is the electron velocity, which is determined by the beam

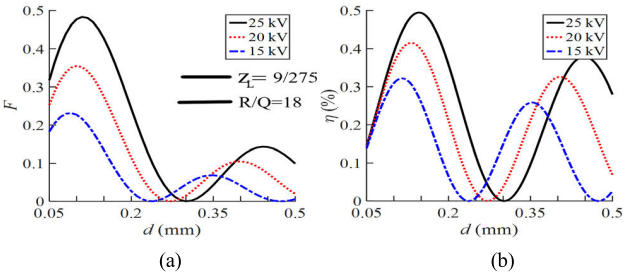

FIGURE 3. (a) Gain bandwidth factor F and (b) efficiency η of a single gap versus the gap length d for different beam voltage V_0.

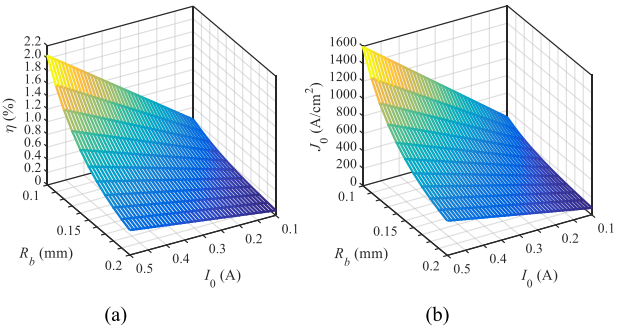

FIGURE 4. (a) Efficiency η of the output cavity with single gap versus the beam current I0 and the beam radius R_b, (b) beam current density J0 versus the beam current I0 and beam radius R_b.

voltage V_0. Thus, the coupling coefficient is a function of the gap length and the electron velocity.

For a bunching cavity, to optimize the gain bandwidth, the gap length should be adjusted to maximize the gain bandwidth factor defined as $F = M\ 2\ (R/Q)$. Assuming that the beam tunnel radius R_t is 0.12 mm and the beam radius R_b is 0.1 mm, the relationship between the gain bandwidth factor F and the gap length d for different beam voltage V_0 is illustrated in Fig. 3(a). The cathode with a larger radius is used to compress to the radius of the electron beam.,and we have mentioned it in our design. The gain bandwidth factor can be improved by raising the beam voltage, and the gap length corresponding to the maximum value is larger. For an output cavity, the gap length should be optimized to the highest efficiency. The efficiency η of the output cavity with a single gap can be estimated by

$$\eta = \frac{\overline{P_{out}}}{P_{in}} = m\frac{M^2 i_1^2 Z_L}{I_0 V_0}\frac{Q_0}{Q_0 + Q_{ext}} \tag{3}$$

where

$$\begin{cases} Z_L = \dfrac{(R/Q)\,Q_L}{1 + jQ_L\left(\omega/\omega_r - \omega_r/\omega\right)} \\ Q_L = \dfrac{1}{1/Q_0 + 1/Q_{\text{ext}}} \end{cases}. \tag{4}$$

where: Z_L is the gap impedance; Q_L is the loaded quality factor; Q_0 is the intrinsic quality factor; Q_{ext} is the external quality factor; I_0 is the DC beam current of individual beam; i_1 is the fundamental component of the induced current, it can generally reach 1.4 to 1.7 times of the I_0 for multi-stage bunching; m is the number of beams, in this paper, m is equals to 10. Assuming that $Q_{ext} = Q_0, I_0 = 0.1\,A, i_1 = 1.5I_0, R_t = 0.12$ mm, $R_b = 0.1$ mm, the relationship between the efficiency η and the gap length d for different beam voltage V_0 is given in Fig. 3(b). Similar to Fig. 3(a), the efficiency is improved by raising the beam voltage, and the optimum gap length increases with the beam voltage.

However, the high beam voltage may lead to the breakdown of electron gun because of the small dimensions at THz band. Therefore, our EIK operates with the beam voltage of 20 kV, then the optimum gap length of the bunching cavity is 0.11 mm and that of the output cavity is 0.13 mm, as shown in Fig. 3(a) and Fig. 3(b), respectively.

However, in order to balance the efficiency and bandwidth, and considering the deviation of theoretical calculation, the gap length of all the cavities are optimized to 0.12 mm by P- IC simulation. If the operating beam voltage is determined, the period length L of the coupled cavity can be calculated by

$$L = \frac{\phi v_p}{2\pi f} \tag{5}$$

where φ is the phase shift of field, and $\varphi = 2\pi$ when the coupled cavity operates at 2π mode; v_p is the phase velocity of field. We make v_p equal to v_0, and the beam voltage at this condition is called synchronous voltage.

B. BEAM PARAMETERS

In theory, the gap coupling coefficient is largest if the beam radius R_b equals to the beam tunnel radius R_t. However, to prevent electrons bombard on the walls of the beam tunnels, the ratio of R_b and R_t need to be restricted. If the beam voltage V_0 is 20 kV, assuming $R_b = 0.83$Rt, $i_1 = 1.5I_0$, d = 0.13mm, the relationship between the estimated efficiency η of the output cavity, the beam current I_0 and the beam radius R_b is given in Fig. 4(a), the relationship between the current density J_0 of beam, the beam current and the beam radius is given in Fig. 4(b). Fig. 4(a) indicates that the efficiency can be improved by increasing the beam current or decreasing the beam radius, but at the expense of an evident increase in current density of beam, as shown in Fig. 4(b). To achieve an efficiency of 1.5%, the current density of beam needs to exceed 1000 A/cm^2. Besides, the radius of the beam tunnel should be small enough to cut off the propagation of electromagnetic wave in the tunnel while accommodating the electron beam with an appropriate current density. Therefore, the electron beam with small diameter and high current density is the key to improve the output power and efficiency of devices.

The cold cathode based on the field emission principle has an extremely high current density [16], [17], but the total current is low, and there are other problems such as inconsistent electron velocity and low reliability, thus, the thermalcathode with high current density is more appropriate for some time to come. Recently, high emission current density of up to

50-100 A/cm^2 have been achieved with a meaningful life by thermal cathode in the experiment [18], [19]. Besides, for the high power klystrons, a conventional approach is to use magnetic field compression to improve the beam current densities to over 100 A/cm^2. However, a high compression ratio requires a strong magnetic field of the focus system. The most advanced designs have the ability to focus a 100 mA thermal beam through a tunnel diameter of 0.125 mm [6]. After considering various factors comprehensively, the parameters of both electron beams are set as $V_0 = 20$ kV, $I_0 = 0.1$ A, $R_b = 0.1$ mm,and $R_t = 0.12$ mm, thus the current density of the electron beam is $J_0 = 318$ A/cm^2, which is feasible for the thermal beam with high emission current density and low compression ratio (<20). However, the efficiency is only 0.4 % under this condition according to Fig. 4(a), thus the efficiency single gap is difficult to be improved because of the limitation of beam current.

C. MULTI-EXTRACTION OUTPUT CAVITY

If the multi-gap coupled cavity operates at the 2π-mode, the characteristic impedance is proportional to the number of gaps, thus, it is an effective approach to improve the power and efficiency of devices. Referring to the research of [15], and introducing the radial coupling coefficient (M_r), the square of the multi-gap coupling coefficient can be defined as

$$M^2 = \frac{M_z^2 M_r^2}{N^2}\left[N + 2\sum_{n=1}^{N}(N-n)\cos(n\beta_e L)\right] \quad (6)$$

where: N is the number of gaps, and the value of $\beta_e L$ is an integral multiple of 2π when the cavity operates at 2π mode. Fig. 5(a) gives the square of the multi-gap coupling coefficient M versus the beam voltage V_0. Around the synchronous voltage of 20 kV, the value of M^2 for different number N of gaps tends to a fixed value, which is equal to the coupling coefficient of a single gap. However, when the beam voltage deviates from the synchronous voltage, the variation of M^2 is more significant with the increase of N. Actually, the electrons lose part of kinetic energy and slow down when they pass through the gap, which is equivalent to the drop in beam voltage. The estimated efficiency η of the output cavity versus the number N of gaps is given in Fig. 5(b). Benefited with the linear growth of the R/Q of coupled cavity, the efficiency is improved significantly with the increase of the number of gaps, but ultimately saturates because of the decrease in M^2 caused by the deceleration of electrons. Therefore, it is meaningless to increase the number of gaps without restriction. Besides, increasing the number of gaps may cause the mode competition.

To overcome the above problem that a single multi-gap output cavity cannot extract energy from the beam efficiently, a multi-extraction output cavity is proposed, as shown in Fig. 6. The energies of beams are extracted twice by two $TM_{10,1,0}$ mode coaxial coupled cavities with five periods, and the output power signals are superimpose in the same

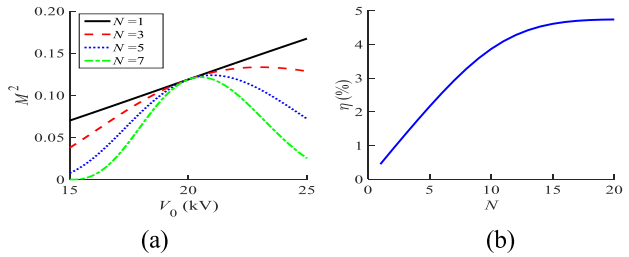

FIGURE 5. (a) Square of the multi-gap coupling coefficient M for different number N of gaps, (b) efficiency η of output cavity versus the number N of gaps.

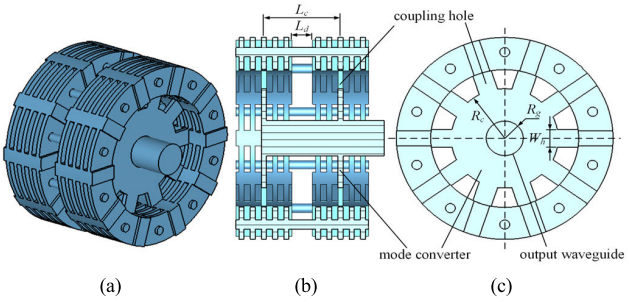

FIGURE 6. (a) Sketch of the multi-extraction output circuit, (b) Side view of the multi-extraction output circuit, (c) cross section of the multi-extraction output circuit.

phase by the axial output circuit. The axial output circuit is consisted of the rectangular coupling holes with a width W_h of 0.46 mm, the mode converters with a radius R_c of 1.3 mm and the circular waveguide at TM_{01} mode with a radius R_g of 0.46 mm. The mode converters is used to convert the $TM_{1,0}$ mode in the coupling holes to the $TM_{0,1}$ mode in the circular waveguide, and they connect with the middle gap of each coupled cavity by the coupling holes arranged along the angular direction, which can minimize the distortion of the field pattern in the gaps caused by the output circuit. The heights of the coupling holes and the mode converters are equal to the gap length of 0.12 mm. External quality factor Q_{ext} can be used to characterize the coupling between the cavity and the load, it is calculated by the group delay and given in Fig. 7. For circuit topology, the output ports of two identical output cavities are connected in parallel, thus, the Q_{ext} of multi-extraction output cavity is half that of a single output cavity, as shown in Fig. 7(a). The width of the coupling hole has a significant effect on the external quality factor, as shown in Fig. 7(b), the Q_{ext} decreases with the increase of the W_h, which means that the coupling is improved. Fig.8(a) gives the guide wavelength of the output circular waveguide corresponding to the waveguide radius R_g, and the external quality factor versus the waveguide radius is given in Fig.8(b), and it shows that the Q_{ext} increases with the increase of the R_g.

In order to superimpose the output power signals in the same phase, the phase of the field in each cavity should be identical, and the distance L_c between the middle gaps of each

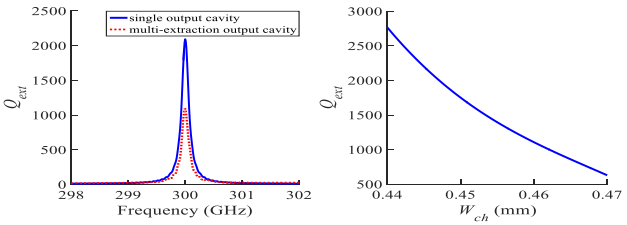

FIGURE 7. (a) External quality factor Qext of output circuit calculated by group delay. (b) External quality factor Qext of multi-extraction outpu circuit versus the width Wh of coupling hole.

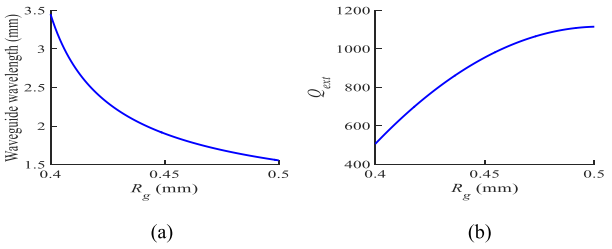

FIGURE 8. (a) Guide wavelength and (b) Q_{ext} of the multi-extraction output cavity versus the waveguide radius R_g of the circular waveguide.

coupled cavity should be equal to the guide wavelength of the output waveguide. From (6), if the electron passes through a period length, the phase shift of the field is 2π, therefore, the drift distance L_d between the coupled cavities should be an integral multiple of the period length, such as 0.544 mm, which is two times of the period length of 0.272 mm. However, the electrons have decelerated as they pass through the first coupled cavity, thus, the L_d is slightly shorted to 0.51 mm according to PIC simulation. Then, we have the value of L_c is 1.87 mm. Thus, the radius of the circular waveguide is set to 0.46 mm from Fig.8(a). According to the circuit theory, the load will obtain the highest power when the Q_{ext} is equal to the Q_0 of 1100, thus, the width of the coupling hole is determined to be 0.46 mm according to Fig.7(b). Benefiting from the flexibility of the same phase by adjusting the distance between the coupled cavities and the guide wavelength of output waveguide, and no additional combiner is needed, which is beneficial to simplify the device.

III. STABILITY ANALYSIS

For the cavity operate in high-order mode, the risk of mode competition could not be ignored because of the numerous resonant modes coexist in the cavity. There are two transverse modes adjacent to the $TM_{10,1,0}$ mode are named as $TM_{9,1,0}$ and $TM_{11,1,0}$ according to the pattern of the axial electric field in the cross section. Moreover, the coupling between cavities induces a sequence of longitudinal resonant modes. For a coupled cavity with the period length

L and the number of periods N, N longitudinal modes are corresponding to the phase shift of the single period

$$\theta = \beta L = \frac{n}{N}\pi, n = 0, 1, 2 \ldots N-1 \qquad (7)$$

where β is the propagation constant of the field. Increasing the number of periods will lead to more resonant modes,

TABLE 2. Frequencies and instantaneous bandwidths of interfering mode.

Mode	f_r (GHz)	Q_0	BW(GHz)
$TM_{9,1,0}$-3/7π	299.2	1320	0.23
$TM_{10,1,0}$-2π	300.0	1100	0.27
$TM_{10,1,0}$-1/7π	301.6	1082	0.28

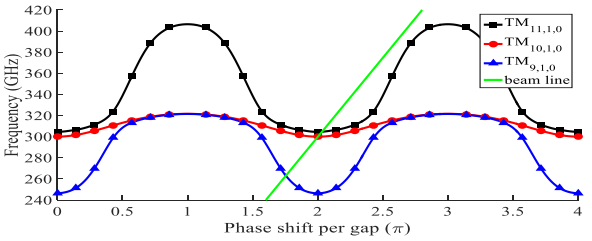

FIGURE 9. Dispersion curves of three adjacent modes and beam line of 20 kV.

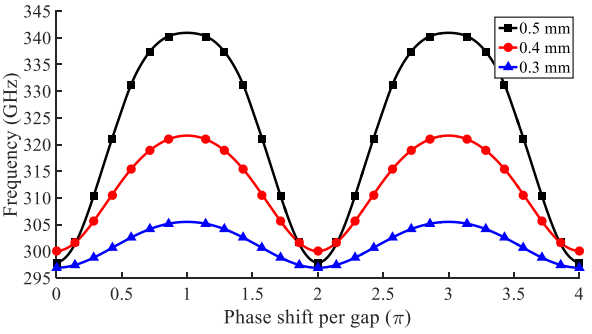

FIGURE 10. Dispersion curves of $TM_{10,1,0}$ mode for different width of coupling tunnel.

resulting in a fairly narrow frequency spacing between some modes. The dispersion characteristic of coupled cavity is an intuitive approach to identify the possibilities of mode competition. As an example, the dispersion curves of the $TM_{10,1,0}$ mode coupled cavity with seven periods is illustrated in Fig. 9. The $TM_{10,1,0} - 1/7\pi$ mode and $TM_{9,1,0} - 3/7\pi$ mode may interfere with the operating mode ($TM_{10,1,0} - 2\pi$) because of the narrow frequency spacing. TABLE 2 gives the resonant frequencies fr and the instantaneous bandwidths BW calculated by the intrinsic quality factor Q_0.

It is clear that the frequency spacing between the operating mode and either of the adjacent modes is wider than the sum of half-bandwidth of the two modes, which confirms that mode competition will not occur when the coupled cavity operating at $TM_{10,1,0} - 2\pi$ mode. The width of the coupling tunnel determines the coupling between the cavities, which affects the dispersion characteristics. The dispersion curves of $TM_{10,1,0}$ mode for different width of the coupling tunnel is given in Fig. 10. With the increase of the width of the coupling channel, the fluctuation of dispersion curve increases, which provides wider spacing of resonant frequency to prevent

mode competition. However, the characteristic impedance will decrease with the increase of the width as a result of more and more electric fields exist in the coupling tunnels, thus the width of the coupling tunnel should be set at a compromise.

The electron beam will exchange energy with the RF field at the resonant modes near the beam line. Fig. 9 indicates that the $TM_{10,1,0}-2\pi$ and the $TM_{11,1,0}-2\pi$ mode exhibit the possibility of generating self-oscillation. Uncontrollable self-oscillation will destroy the pattern of field and disturb the bunching of the electron beam, resulting in the deterioration of gain and stability. To prevent the uncontrollable self-oscillation, the total power loss of the whole interaction circuit must be positive, which is judged by the stability condition expressed as, where G_l is the equivalent circuit conductance of the cavity, G_e is the conductance of the beam [20]. G_l reflects the Joule-loss of the cavities, it is always positive. However, G_e describes the power exchange between the electron beam and the RF field, it is positive when power transferred from the beam to the field is less than that absorbed by the beam, and becomes negative on the contrary. The normalized beam conductance is

$$g_e = \frac{G_e}{G_0} = \frac{\beta_e}{4}\frac{d\,|M|^2}{d\beta_e} \tag{8}$$

where $G_0 = I_0/V_0$ is the DC beam conductance. Thus, the normalized beam conductance is a function of the beam voltage. Substituting (6) into (8),the normalized beam conductance of coupled cavity can be defined as

$$g_e = -\frac{\beta_e}{4N^2}\left\{\frac{d\,|M_z M_r|^2}{d\beta_e}\left[N+\sum_{n=1}^{N}(N-n)\cos(n\beta_e L)\right] + M_2 M_r \sum_{n=1}^{N}\frac{d\,[(N-n)\cos(n\beta_e L)]}{d\beta_e}\right\} \tag{9}$$

where

$$\frac{d\,|M_z M_r|^2}{d\beta_e} = 2\frac{\sin(\theta_d/2)}{\theta_d/2}\frac{I_0^2(\gamma_e R_b)-I_1^2(\gamma_e R_b)}{I_0^2(\gamma_e R_t)} \times\left\{\frac{d\left[\theta_d\cos(\theta_d/2)-2\sin(\theta_d/2)\right]}{\theta_d^2} -\left[\frac{\sin(\theta_d/2)}{(\theta_d/2)}\right]\frac{\beta_e R_t I_1^2(\gamma_e R_t)}{I_0(\gamma_e R_t)}\right\} \tag{10}$$

and

$$\sum_{n=1}^{N}\frac{d\,[(N-n)\cos(n\beta_e L)]}{d\beta_e} = -\sum_{n-1}^{N} n(N-n)\sin(n\beta_e L) \tag{11}$$

Fig. 11(a) gives the g_e of proposed coupled cavity with seven periods at $TM_{10,1,0}-2\pi$ mode and the $TM_{11,1,0}-2\pi$ mode, obviously, the g_e is positive at the operating beam voltage of 20 kV, thus, it is believed that the coupled cavity is stable. Fig. 11(b) indicates that, with the increase of period numbers, the change of G_e becomes more significant.

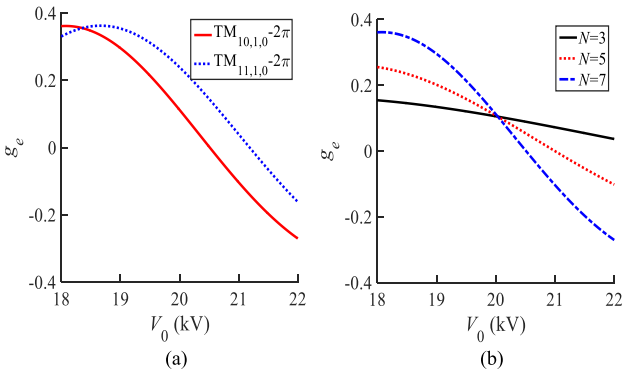

FIGURE 11. Normalized beam conductance G_e versus beam voltage V_0 for (a) the competition modes and (b) the number N of periods.

TABLE 3. Parameters of each cavity.

Cavity	f (GHz)	R/Q (Ω)	M	Q_0	Q_{ext}
input cavity	300	13	0.34	1150	1100
bunching cavity	300	18	0.34	1150	∞
output cavity	300	26	0.34	1100	1100

Besides, the positive range of G_e is reduced with the increase of period numbers. In other words, the coupled cavity with more periods requires a beam voltage with higher precision and stability, otherwise, the g_e will be negative when the beam voltage is slightly higher than the operating voltage.

IV. PIC SIMULATIONS AND ANALYSIS

A. SIMULATION AND RESULTS

The complete interaction circuit of the $TM_{10,1,0}$ mode multi-beam EIK proposed in this paper consists of an input cavity with the same structure as the single output cavity, the bunching section with four bunching cavities and a multi-extraction output cavity containing two identical output cavities, as shown in Fig. 12(a). The conductivity of the cavity material is set to 5.8 × 107 S/m. The synchronous tuning of the cavities is utilized to raise the gain, and the important parameters of each cavity are given in TABLE 3. Same as the conventional klystron, the bunching section of the proposed EIK utilizes variable drift distances to enhance the bunching of the beams. In the case of small signals, the drift distances in the first two sections are approximately one-quarter of the reduced plasma wavelength for the optimal bunching process. To prevent the over bunching, so the drift distances in the next three sections should be shorter, which are determined by the PIC simulation. Finally, the drift distances between the cavities in the bunching section are arranged as 4.5, 4, 2, 2,and 1mm, respectively. Driven by ten individual DC electron beams with the beam voltage V_0 of 20 kV, the beam current I_0 of 0.1A and the beam radius R_b of 0.1 mm, the performances of the proposed multi-beam EIK are demonstrated by the 3D PIC simulation using CST-PIC solver. The minimum focus magnetic field to maintain

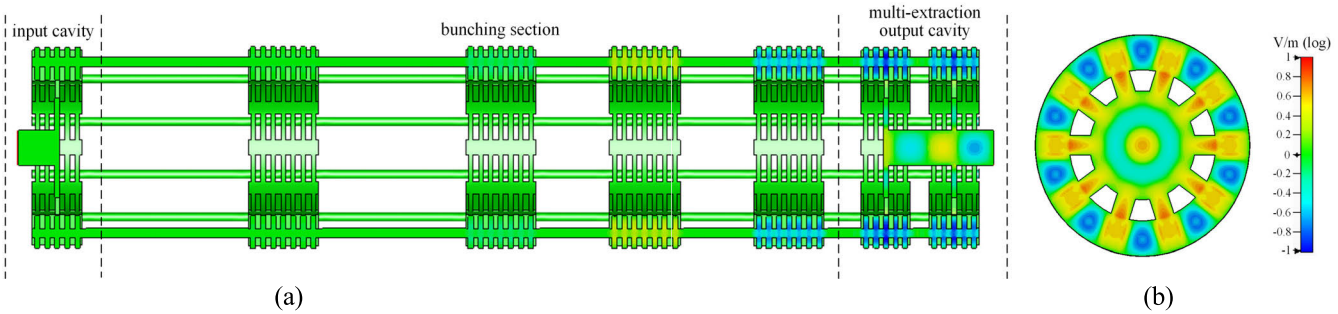

FIGURE 12. (a) Longitudinal section of the model of $TM_{10,1,0}$ mode multi-beam EIK and a snapshot of the normalized axial electric field pattern, (b) a snapshot of the normalized axial electric field pattern at cross sections of the output cavity.

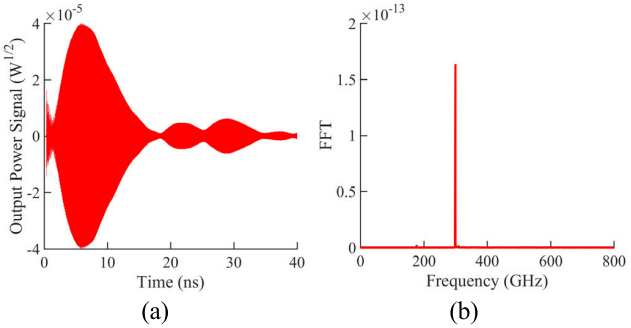

FIGURE 13. (a) The signal of the output power without an RF drive signal of 300 GHz, (b) frequency spectrum of the output signal.

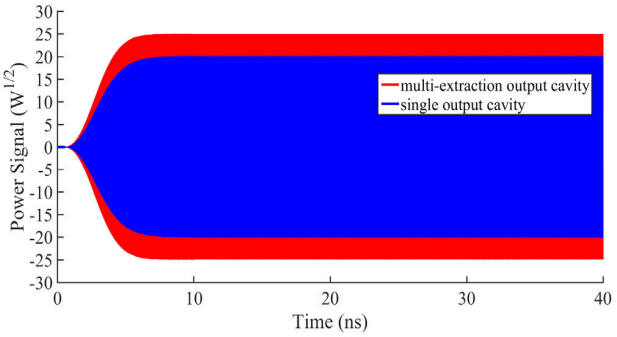

FIGURE 14. Output signal of the EIK with multi-extraction output cavity and the EIK with single output cavity.

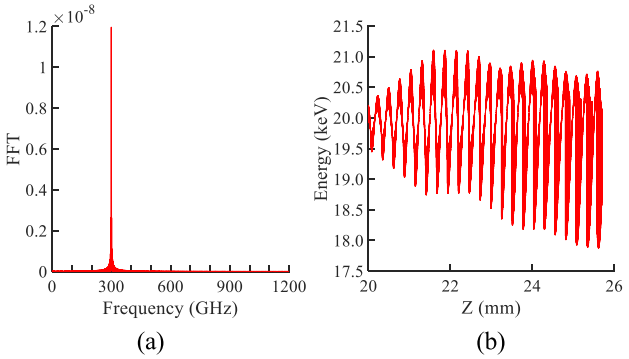

FIGURE 15. (a) Frequency spectrum of output power signal with an RF drive signal of 300 GHz, (b) phase space of electrons in the last cavities.

the focus of the beam called Brillouin field can be given $B_b = 0.83 \times 10^{-3}(I_0)^{1/2}/[R_b(V_0)^{1/4}] = 0.22$T.

The theoretical calculation indicates that the interaction circuit satisfies the stable condition, however, even if there is no input signal, the rising edge of the DC electron beams inevitably excites a weak oscillation signal of the operating mode with a frequency of 300 GHz, as shown in Fig.13. The stable DC electron beams can be regarded as loads of the cavities because of the positive G_e, thus the oscillation will gradually decay and remain a small amplitude, as shown in Fig.13(a). This controllable oscillation of operating mode does not destroy the stability of the device and the quality of the output signal.

The signal with power of 5 mW at desired center frequency of 300 GHz is injected into the device, and a snapshot of normalized axial electric field pattern at longitudinal sections of the whole interaction circuit is shown in Fig. 12(a). The electric field has the same pattern within each gap and becomes stronger cavity by cavity. Fig. 12(b) gives a snapshot of the normalized axial electric field pattern at cross sections of the output cavities. Obviously, the field pattern agrees well with $TM_{10,1,0}$ mode, thus, it is convinced that the device is operating at $TM_{10,1,0} - 2\pi$ mode. The steady output power signal is obtained after 8 ns, as shown in Fig. 14, the saturated output power is $P_{out} = 0.5 \times 25^2$W=312.5W. As a contrast, the $TM_{10,1,0}$ mode multi-beam EIK with a single output cavity is modeled and simulated under the same conditions, and its ouput power signal is also given in Fig. 14.

Obviously, the maximum output power of the EIK with a multi-extraction output cavity is nearly twice that of the EIK with a single output cavity. Therefore, the multi-extraction output cavity has been proven to improve the efficiency of EIK significantly. The frequency spectrum of the output signal is very pure within a wide band, as shown in Fig.15(a), which signifies that no model competition occurred. Therefore, the correctness of stability analysis in Sec. III is proved. Fig.15(b) shows the phase space of the electrons in the last bunching cavity and the multi-extraction output cavity. The

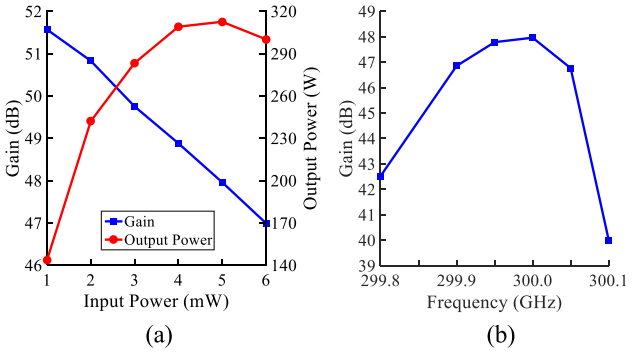

FIGURE 16. (a) Gain curves of the input power at 300 GHz and (b) frequency with an input power of 5 mW.

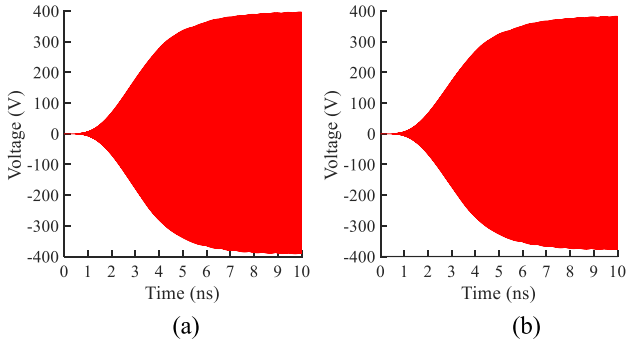

FIGURE 17. (a) Voltage of the middle gap of the first output cavity, (b) voltage of the the junction between the coupling hole and the coupled cavity.

stepwise enhanced modulation of the beam is observed, and most electrons drastically decelerate in the output cavity, indicating that the energy of electrons is converted to the electromagnetic fields and coupled to the load. The gain curve of the input power and frequency is shown in Fig. 16. The maximum output power of 312.5 W is obtained for an input power of 5 mW at the center frequency of 300 GHz yielding a gain of 48 dB, and the 3-dB gain bandwidth calculated from Fig. 16(b) is about 200 MHz.

B. POWER CAPACITY ANALYSIS

The simulation results show that the proposed EIK has good performances, however, the device may not be able to withstand such large power because of the small size dimension and the restrictions of surface roughness. A strong electric field may lead to the breakdown of narrow gaps. According to the PIC simulation, the axial electric field in the middle gap of the first output cavity is strongest, and the voltage of the gap is given in Fig. 17(a), the voltage will increase to 397 V over time. The coupling holes can be regarded as the rectangular waveguides with a sectional dimension of 0.46 mm $\times$ 0.12 mm, and it is cut-off for the electromagnetic waves at 300 GHz. Complex reflection exists at the junction between the coupling hole and the coupled cavity, thus, it is difficult to calculate the power capacity of the coupling holes theoretically. But the voltage of the junction can be obtained by PIC simulation conveniently, as shown in Fig. 17(b), the voltage will increase to 380 V over time. Ideally, the electric field strength of the breakdown limit called E_{br} is up to 1.3 MV/cm in the vacuum, however, because of the limitation of process conditions, the actual E_{br} is much smaller. According to the research of *R*.

Hawley *et al.* [21], a conservative E_{br} of 100 kV/cm is reasonable. Thus, the breakdown voltage of the gap with a length of 0.12 mm is 1.2 kV, which is much higher than 397 V and 380V, thus, the risk of gap breakdown is very low in the proposed EIK.

The power capacity of output circular waveguide operating at $TM_{0,1}$ mode is defined as

$$P_{br} = \frac{\pi E_{br}^2 R_g^2}{2Z_{TM}} \tag{12}$$

where Z_{TM} is the wave impedance of $TM_{0,1}$ mode, R_g is the radius of the waveguide. Then we have the power capacity of the output circular waveguide at $TM_{0,1}$ mode is 160 kW, which is much higher than the maximum output power of 312.5 W. Synthesize the analysis above, it is believed that the power capacity of the proposed EIK is enough.

V. CONCLUSION

Conventional EIK is facing a series of difficulties when it extends to the THz band, the most prominent of which is the rapidly reduced dimension and the higher requirement of the current density of the electron beam. To deal with these problems, a novel $TM_{10,1,0}$ mode multi-beam extended interaction klystron is proposed in this paper, and the interaction circuit including the coaxial coupled cavity and the multi-extraction output cavity are designed and analyzed, and the crucial structure parameters are determined. The $TM_{10,1,0} - 2\pi$ mode is determined as the operating mode for larger dimensions and higher R/Q. There are ten electron beams are formatted with the voltage of 20 kV and the overall current of 1 A (0.1 A $\times$ 10), and the current density of each beam is 318 A/cm^2, which is easily achieved by the electron gun that using thermal cathode with low compression ratio. The results of the 3D PIC simulation confirm that the device works at the $TM_{10,1,0} - 2\pi$ mode without mode competition and self-oscillation, and the modulation of the beams is intense. The maximum output power is 312.5 W with a gain of up to 48 dB at the center frequency of 300 GHz, the 3-dB gain bandwidth of 200 MHz is relatively narrow because of the high *Q*-factor cavities and the synchronous tuning. The results of PIC simulation indicate that the multi-extraction output cavity can significantly improve the output power and efficiency. The power capacity of the interaction circuit is also analyzed briefly, the results indicate that the power capacity has a lot of margins. In summary, the $TM_{10,1,0}$ mode multi-beam EIK proposed in this paper provides a great potential approach for developing the high power terahertz sources.

REFERENCES

[1] A. Roitman, R. Dobbs, D. Berry, M. Hyttinen, P. Horoyski, and B. Steer, "Advantages of the extended interaction klystron technology at millimeter and sub-millimeter frequencies," in *Proc. IEEE Pulsed Power Plasma Sci. Conf.*, vol. 2, Jun. 2007, pp. 1049–1053, doi: 10.1109/PPPS.2007.4345972.

[2] A. Roitman, P. Horoyski, R. Dobbs, and D. Berry, "Space-borne EIK technology," in *Proc. IEEE Int. Vac. Electron. Conf.*, Apr. 2014, pp. 211–212, doi: 10.1109/IVEC.2014.6857565.

[3] R. Dobbs, M. Hyttinen, and B. Steer, "A 48 GHz, 500 W CW extended interaction klystron," in *Proc. IEEE 14th Int. Vac. Electron. Conf. (IVEC)*, May 2013, pp. 2–3, doi: 10.1109/IVEC.2013.6570924.

[4] A. Roitman, D. Berry, and B. Steer, "State-of-the-art W-band extended interaction klystron for the CloudSat program," *IEEE Trans. Electron Devices*, vol. 52, no. 5, pp. 895–898, May 2005, doi: 10.1109/TED.2005.845799.

[5] J. H. Booske, R. J. Dobbs, C. D. Joye, C. L. Kory, G. R. Neil, G.-S. Park, J. Park, and R. J. Temkin, "Vacuum electronic high power terahertz sources," *IEEE Trans. Terahertz Sci. Technol.*, vol. 1, no. 1, pp. 54–75, Sep. 2011, doi: 10.1109/TTHZ.2011.2151610.

[6] D. Berry, H. Deng, R. Dobbs, P. Horoyski, M. Hyttinen, A. Kingsmill, R. MacHattie, A. Roitman, E. Sokol, and B. Steer, "Practical aspects of EIK technology," *IEEE Trans. Electron Devices*, vol. 61, no. 6, pp. 1830–1835, Jun. 2014, doi: 10.1109/TED.2014.2302741.

[7] R. Dobbs, A. Roitman, P. Horoyski, M. Hyttinen, D. Sweeney, D. Chernin, M. Blank, N. S. Barker, J. Booske, E. Wright, J. Calame, and O. V. Makarova, "Fabrication techniques for a THz EIK," in *Proc. IEEE Int. Vac. Electron. Conf. (IVEC)*, May 2010, pp. 181–182, doi: 10.1109/IVELEC.2010.5503544.

[8] Y. M. Shin, L. R. Barnett, and N. C. Luhmann, "MEMS-fabricated micro vacuum electron devices (μVEDs) for terahertz (THz) applications," in *Proc. 33rd Int. Conf. Infr. Millim. Waves 16th Int. Conf. Terahertz Electron.*, Sep. 2008, pp. 1–3, doi: 10.1109/ICIMW.2008.4665430.

[9] D. Wang, G. Wang, J. Wang, S. Li, P. Zeng, and Y. Teng, "A high-order mode extended interaction klystron at 0.34 THz," *Phys. Plasmas*, vol. 24, no. 2, Feb. 2017, Art. no. 023106, doi: 10.1063/1.4975649.

[10] G. X. Shu, H. Yin, L. Zhang, J. P. Zhao, G. Liu, A. D. R. Phelps, A. W. Cross, and W. He, "Demonstration of a planar *W*-band, kW-level extended interaction oscillator based on a pseudospark-sourced sheet electron beam," *IEEE Electron Device Lett.*, vol. 39, no. 3, pp. 432–435, Mar. 2018, doi: 10.1109/LED.2018.2794469.

[11] J. Pasour, E. Wright, K. T. Nguyen, A. Balkcum, F. N. Wood, R. E. Myers, and B. Levush, "Demonstration of a multikilowatt, solenoidally focused sheet beam amplifier at 94 GHz," *IEEE Trans. Electron Devices*, vol. 61, no. 6, pp. 1630–1636, Jun. 2014, 10.1109/TED.2013.2295771.

[12] J. Pasour, K. Nguyen, E. Wright, A. Balkcum, J. Atkinson, M. Cusick, and B. Levush, "Demonstration of a 100-kW solenoidally focused sheet electron beam for millimeter-wave amplifiers," *IEEE Trans. Electron Devices*, vol. 58, no. 6, pp. 1792–1797, Jun. 2011, doi: 10.1109/TED.2011.2126577.

[13] Y. Yin, F. Zeng, B. Wang, H. Li, L. Bi, Z. Chang, R. Peng, S. Zhu, C. Xu, and L. Meng, "Preliminary study of a multiple-beam extended-interaction oscillator with coaxial structure," *IEEE Trans. Electron Devices*, vol. 65, no. 6, pp. 2108–2113, Jun. 2018, doi: 10.1109/TED.2018.2797924.

[14] S. Lu, C. Zhang, S. Wang, and Y. Wang, "Stability analysis of a planar multiple-beam circuit for *W*-band high-power extended-interaction klystron," *IEEE Trans. Electron Devices*, vol. 62, no. 9, pp. 3042–3048, Sep. 2015, doi: 10.1109/TED.2015.2435031.

[15] K. Zhang, Z. Wu, and S. Liu, "Study of an extended interaction oscillator with a rectangular reentrance coupled-cavity in terahertz region," *J. Infr., Millim., Terahertz Waves*, vol. 30, no. 4, pp. 309–318, Apr. 2009, doi: 10.1007/s10762-008-9456-4.

[16] J. A. Nation, L. Schachter, F. M. Mako, L. K. Len, W. Peter, C.-M. Tang, and T. Srinivasan-Rao, "Advances in cold cathode physics and technology," *Proc. IEEE*, vol. 87, no. 5, pp. 865–889, May 1999, doi: 10.1109/5.757258.

[17] K. B. K. Teo, E. Minoux, L. Hudanski, F. Peauger, J. Schnell, L. Gangloff, P. Legagneux, D. Dieumegard, G. A. J. Amaratunga, and W. I. Milne, "Carbon nanotubes as cold cathodes," *Nature*, vol. 437, no. 7061, pp. 967–968, 2005, doi: 10.1038/437968a.

[18] J. Zhao, N. Li, J. Li, L. R. Barnett, M. Banducci, D. Gamzina, Z. A. Munir, and N. C. Luhmann, "High current density and long-life nanocomposite scandate dispenser cathode fabrication," *IEEE Trans. Electron Devices*, vol. 58, no. 4, pp. 1221–1228, Apr. 2011, doi: 10.1109/TED.2011.2109723.

[19] Y. Yang, Y. Wang, W. Liu, Z. Pan, J. Li, and J. Wang, "Robustness investigation on nanosized-scandia-doped dispenser cathodes," *IEEE Trans. Electron Devices*, vol. 65, no. 6, pp. 2072–2076, Jun. 2018, doi: 10.1109/TED.2018.2814542.

[20] F.-M. Lin and X.-P. Li, "Monotron oscillation in double-gap coupling output cavities of multiple-beam klystrons," *IEEE Trans. Electron Devices*, vol. 61, no. 4, pp. 1186–1192, Apr. 2014, doi: 10.1109/TED.2014.2303133.

[21] R. Hawley, A. A. Zaky, and E. Z. Eldine, "Insulating properties of high vacuum," *Proc. Inst. Electr. Eng.*, vol. 112, no. 6, p. 1237, 1965, doi: 10.1049/piee.1965.0207.

[22] G. M. Branch, "Electron beam coupling in interaction gaps of cylindrical symmetry," *IRE Trans. Electron Devices*, vol. 8, no. 3, pp. 193–207, May 1961, doi: 10.1109/T-ED.1961.14787.

FU-MIN LIN was born in 1964. He received the Ph.D. degree from the Institute of Electrics, Chinese Academy of Sciences, in 2003. He is currently a Professor and an Instructor of graduate students with the School of Physics and Optoelectronic Engineering, Guangdong University of Technology, Guangdong, China. His research interests include high-power microwave devices, microwave filters and RF circuits, and antenna.

SHUNING WU was born in 1997. He received the B.E. degree from the School of Physics and Optoelectronic Engineering, Guangdong University of Technology, Guangdong, China, where he is currently pursuing the M.S. degree in electronic science and technology. His research interests include klystron, antenna, and RF circuits.

YUJIE XIAO was born in 1993. He received the B.E. degree from the School of Physics and Optoelectronic Engineering, Guangdong University of Technology, Guangdong, China, where he is currently pursuing the M.S. degree in electronic science and technology. His research interests include klystron and RF circuits.

LIANGXIAN ZHANG was born in 1996. He received the B.E. degree from the School of Physics and Optoelectronic Engineering, Guangdong University of Technology, Guangdong, China, where he is currently pursuing the M.S. degree in electronic science and technology. His research interests include antenna and RF circuits.